Journal of Zhejiang University-SCIENCE B (Biomedicine & Biotechnology) 2021 22(11):966-970
www.jzus.zju.edu.cn; www.springer.com/journal/11585
E-mail: jzus_b@zju.edu.cn

Correspondence
https://doi.org/10.1631/jzus.B2100407

Check for updates

Response of *Escherichia coli* to hydrogen nanobubbles: an in vitro evaluation using synchrotron infrared spectroscopy

Jinfang LU[1,2,5*], Jin ZHENG[1,2,5*], Yadi WANG[3], Jie CHENG[2], Xueling LI[4], Jun HU[1,2], Bin LI[1,2✉], Junhong LÜ[1,2✉]

[1]CAS Key Laboratory of Interfacial Physics and Technology, Shanghai Institute of Applied Physics, Chinese Academy of Sciences, Shanghai 201800, China
[2]Shanghai Advanced Research Institute, Chinese Academy of Sciences, Shanghai 201203, China
[3]College of Pharmacy, Binzhou Medical University, Yantai 264003, China
[4]National Engineering Research Center for Nanotechnology, Shanghai 201318, China
[5]University of Chinese Academy of Sciences, Beijing 100049, China

Hydrogen (H_2)-rich water, an apparent source of molecular H_2, is an emerging functional drink with many purported benefits for human health (Yang et al., 2020; Ostojic, 2021). The preventive and therapeutic effects of H_2 on various pathological processes have been intensively investigated in numerous clinical trials; it is commonly believed that the beneficial effects are mainly attributed to its selective antioxidant and anti-inflammatory properties (Lee et al., 2015; Ohta, 2015; LeBaron et al., 2019; Qiu et al., 2020). In recent years, a handful of rodent studies revealed that exogenous H_2 can affect the gut microbiota (Sha et al., 2018; Valdes et al., 2018). For example, H_2 was reported to induce a higher abundance of butyrate-producing bacteria in a rat model of Parkinson's disease (Bordoni et al., 2019). Recent first-in-human trials have explored the effects of the long-term consumption of H_2-rich water on antioxidant activity and the gut flora (Sha et al., 2018; Suzuki et al., 2018). Although these promising results suggest that the intestinal microbiota may be another plausible target for molecular H_2, more studies are highly warranted to explain the mechanism(s) of H_2 action on bacterial growth and functions.

✉ Junhong LÜ, lujunhong@zjlab.org.cn
Bin LI, libin@sinap.ac.cn
* The two authors contributed equally to this work
Junhong LÜ, https://orcid.org/0000-0003-2873-3137
Bin LI, https://orcid.org/0000-0002-8348-7445

Received May 9, 2021; Revision accepted Aug. 7, 2021; Crosschecked Oct. 14, 2021

Fourier transform infrared (FTIR) spectroscopy can provide the chemical composition information of samples with the advantages of high sensitivity and good reproducibility (Wang et al., 2017). With the technological advance of synchrotron light source, the higher brightness and smaller source spot size have allowed the FTIR spectra to have higher intensity and better signal-to-noise ratio. As the spectral bands contain molecular fingerprint information, FTIR spectroscopy exhibits sufficient specificity to establish the molecular differences of cells exposed to various types of stimulations or treatments. The changes of absorption bands, such as those in position or intensity, reflect the component differences. Thanks to this advantage, FTIR spectroscopy has been widely used in the field of microbiology, especially for studying the changes of microbial constituents under stress conditions (Alvarez-Ordóñez et al., 2011). For example, synchrotron infrared spectroscopy has been employed to study the response of *Escherichia coli* to heat, cold, and ethanol, as well as the interaction between bacteria and metal ions (Hu et al., 2016).

In this study, the effect of H_2 nanobubbles (NBs) on the viability of *E. coli* was first tested by measuring the bacterial growth curve. Compared with double distilled water (dd-water) and nitrogen (N_2) NBs, the growth curve of H_2 NB treatment group did not show any significant changes (Fig. 1a). The colony number of live bacteria during the exponential growth phase was further counted on the culture plates. After culture for 8 h, the counts were 5.5×10^9 and 5.9×10^9 CFU/mL

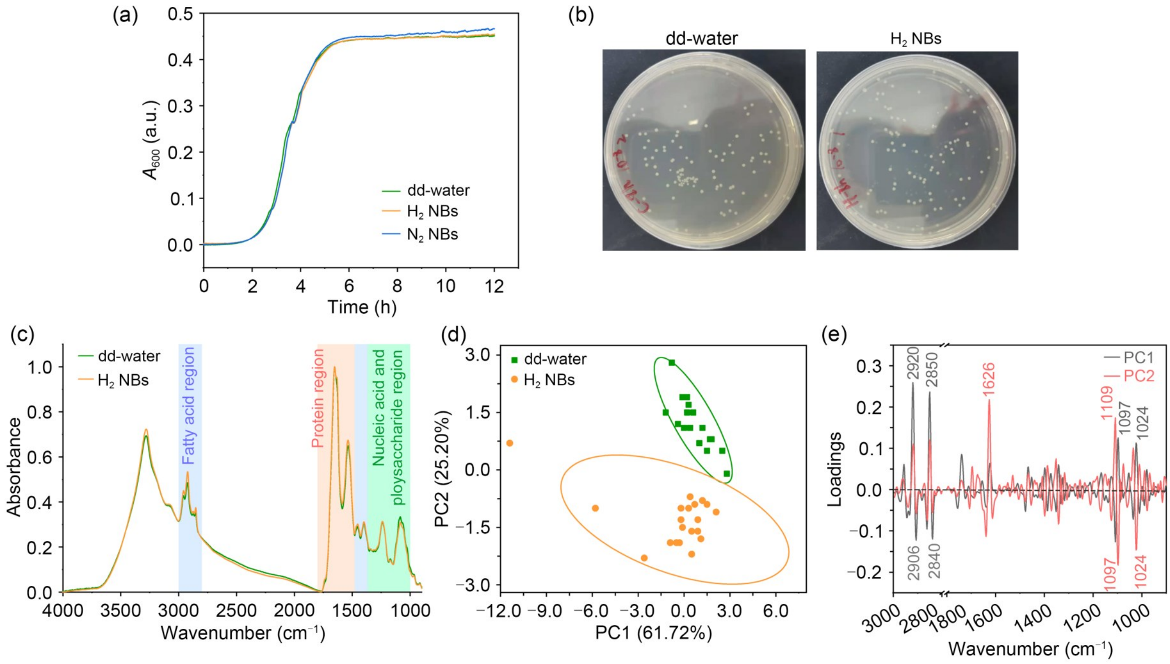

Fig. 1 Effects of hydrogen (H_2) nanobubbles (NBs) on *Escherichia coli*. (a, b) The growth curves (a) and plate photos (b) of *E. coli* subjected to H_2 NB and nitrogen (N_2) NB treatments compared with the double distilled water (dd-water) treatment group; (c) The averaged Fourier transform infrared (FTIR) spectra of bacteria, with the fatty acid regions (3000–2800 cm^{-1} and 1480–1340 cm^{-1}), protein region (1760–1480 cm^{-1}), and nucleic acid and polysaccharide region (1350–1000 cm^{-1}) indicated on the graph; (d) Principal component analysis (PCA) on the second derivative spectra (3000–2800 cm^{-1} and 1800–900 cm^{-1}) of bacteria, with the ellipse representing 95% confidence interval (CI); (e) Loading values of the first two principal components (PCs) within the wavenumber ranges (3000–2800 cm^{-1} and 1800–900 cm^{-1}). A_{600}: absorbance at 600 nm; a.u.: arbitrary unit.

(CFU: colony forming units) for the H_2 NB treatment group and dd-water group, respectively (Fig. 1b), indicating no noticeable effects of H_2 on the vitality and proliferation of *E. coli* in vitro.

Synchrotron FTIR spectroscopy was further conducted to explore whether H_2 NB treatment induces the biochemical component changes of bacterial cells. A total of 20 spectra obtained from the bacterial samples exposed to dd-water or H_2 NBs were collected and analyzed. As shown in Fig. 1c, the differences between the average spectra of the two groups of cells were negligible. To differentiate the component alterations, the second derivative spectra were processed and principal component analysis (PCA) was carried out. The PCA results and loading plots in the whole regions of 3000–2800 cm^{-1} and 1800–900 cm^{-1} are shown in Figs. 1d and 1e. The results showed a variance between the spectra of H_2 NB and dd-water treatment groups of *E. coli* within the 95% confidence interval (CI) (Fig. 1d), which indicated that the chemical components of *E. coli* changed significantly with the existence of H_2 NBs. The loading plots of PC1 (61.72%) and PC2 (25.20%) showed that the bands 2920, 2850, 1626, 1109, 1097, and 1024 cm^{-1} had the largest contribution (Fig. 1e). Notably, the cellular effect of H_2 NBs was also distinct with N_2 NBs, and the latter could not induce remarkable spectral changes (data not shown), suggesting a specific effect and molecular mechanism of H_2 NBs on bacterial cells.

In order to investigate which chemical component exhibited significant change, the infrared band shifts of second-derivative spectra were analyzed in detail. The significantly shifted spectral bands were marked with arrows in Fig. 2a and also listed in Table 1. The results showed that after the H_2 NB treatment, some infrared bands of the bacteria in the Amides I and II regions (1694.14, 1656.00, and 1544.85 cm^{-1}) shifted to higher wavenumbers; several spectral bands corresponding to C–H vibrations of fatty acid components (2921.23, 2851.95, 1467.84, and 1452.17 cm^{-1}) shifted to lower wavenumbers; and the P=O asymmetric stretching vibration band of nucleic acid at 1243.18 cm^{-1} also shifted, as well as the C–O–C vibrations of carbohydrates at 1123.29 and 1057.68 cm^{-1}. The band

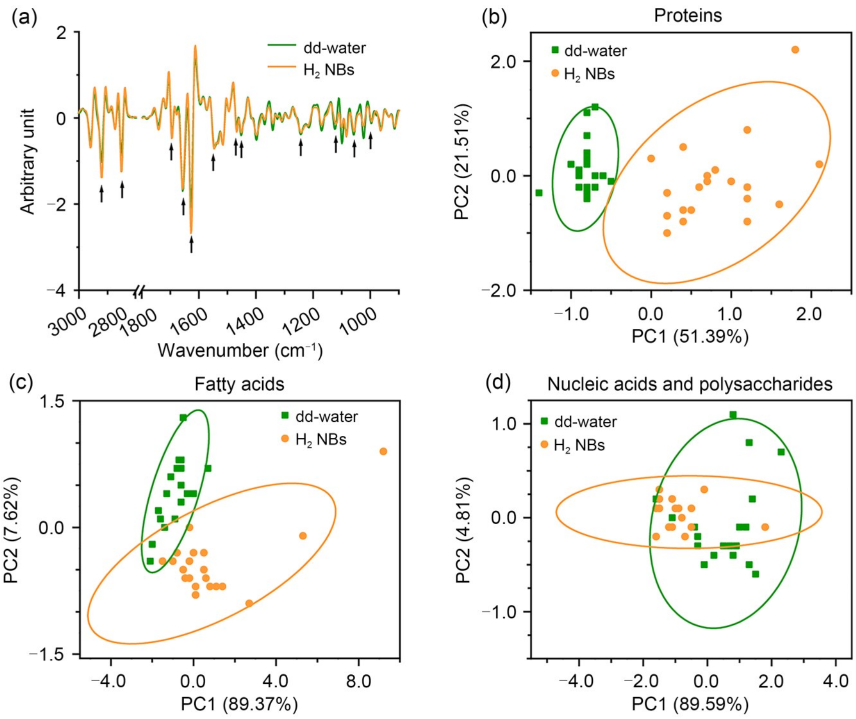

Fig. 2 Nanobubbles (NBs)-induced chemical component changes of *Escherichia coli*, as characterized by Fourier transform infrared (FTIR) spectroscopy. (a) Averaged second-derivative FTIR spectra of *E. coli* subjected to double distilled water (dd-water) and hydrogen (H_2) NB treatments, with the spectral bands with significant shifts indicated with arrows; (b–d) Principal component analysis (PCA) on the second-derivative spectra within the spectral regions 1760–1480 cm^{-1} (proteins, b), 3000–2800 and 1480–1340 cm^{-1} (fatty acids, c), and 1350–1000 cm^{-1} (nucleic acids and polysaccharides, d), with the ellipse representing 95% confidence interval (CI).

Table 1 Infrared band comparison of *E. coli* treated with dd-water and H_2 NBs

Functional group	Wavenumber (cm^{-1})	
	dd-water	H_2 NBs
v_{as}(C–H) of >CH_2 in fatty acids	2921.23±0.41	2920.66±0.52*** ↓
v_s(C–H) of >CH_2 in fatty acids	2851.95±0.22	2851.45±0.32*** ↓
Amide I	1694.14±0.23	1694.47±0.09*** ↑
	1656.00±0.22	1656.45±0.49*** ↑
	1627.19±0.23	1626.89±0.38** ↓
Amide II	1544.85±1.30	1546.81±0.50*** ↑
C–H deformation of >CH_2	1467.84±0.21	1467.51±0.18*** ↓
>CH_2 bending	1452.17±0.31	1451.79±0.21*** ↓
v_{as}(P=O) of >PO_2^- phosphodiesters	1243.18±0.52	1241.89±0.96*** ↓
C–O–C and C–O dominated by ring vibrations of	1123.29±0.88	1119.58±1.25*** ↓
carbohydrates C–O–P and P–O–P	1057.68±0.99	1056.58±0.56*** ↓

v_s: symmetric stretching vibration; v_{as}: asymmetric stretching vibration; dd-water: double distilled water; H_2 NBs: hydrogen nanobubbles. The values are represented as mean±standard deviation (SD) for each group (n=20). The up (down) arrow represents the increase (decrease) of the wavenumber of absorption peak, which corresponds to the blue (red) shift. Comparisons are performed by hypothesis testing through a two-sample t-test. ** and *** denote the degree of significance as P<0.01 and P<0.001, respectively.

shifts of the two spectra indicated that chemical component differences in bacterial cells had taken place following exposure to H_2 NBs, and these differences could be detected by synchrotron FTIR spectroscopy. To intuitively reflect the bacterial component variations, PCA was further performed on the spectral protein region (1760–1480 cm^{-1}; Fig. 2b), fatty acid region (3000–2800 cm^{-1} and 1480–1340 cm^{-1}; Fig. 2c), and nucleic acid and polysaccharide region (1350–1000 cm^{-1}; Fig. 2d). From the PCA diagrams, we could establish that both the protein and fatty acid compositions varied dramatically, while the nucleic acid and polysaccharide compositions showed no significant variations. These results indicated that the effects of H_2 NBs on bacterial cells mainly acted on the protein and fatty acid components.

Since H_2 gas is considered to act as a selective antioxidant, we investigated whether its cellular effect would be comparable with that of natural antioxidant tannins. To this end, bacterial cells were treated with different concentrations of tannins and measured by infrared spectroscopy. As shown in Fig. 3a, tannins at 0.5 g/L had no noticeable effect on bacterial growth (indicated in purple), similarly to the effect of H_2. These cells treated with tannin and H_2 NB-tannin mixture were used to obtain FTIR spectra. The averaged FTIR absorption spectra of these four groups of bacteria are shown in Fig. 3b, which showed that the band positions and strength of tannin and H_2 NB-tannin treatment groups were significantly different from the untreated and H_2 NB treatment groups of bacteria. The corresponding second-derivative spectra are shown in Fig. 3c, where the significantly shifted bands of the tannin or H_2 NB-tannin treatment group were labeled with arrows. PCA on full spectral regions (3000–2800 cm^{-1} and 1800–900 cm^{-1}) could not well discriminate the tannin treatment and the H_2 NB-tannin co-treatment groups (Fig. 3d). The loading plots of PC1 and PC2 are presented in Fig. 3e. However, PCA on the protein region showed significant differences between the tannin treatment group (purple) and the co-treatment group (blue) (Fig. 3f), while the fatty acid and nucleic acid and polysaccharide components were not clearly distinguishable (Figs. S1–S3). These results suggested that H_2 might have a distinct mechanism of action beyond acting as an antioxidant.

In conclusion, we have expanded the application of FTIR to evaluate the cellular effects of H_2 NBs on the model bacterium *E. coli*. The obtained results revealed that molecular H_2 mainly induces the cellular changes in protein and fatty acid compositions in vitro, indicating that the possible direct target of H_2 lies on the membrane. Given the fact that different effects of H_2 NBs on bacterial cells were observed compared with natural antioxidant tannins and the results of our previous report on the binding of H_2 gas to the hydrophobic sites of proteins (Cheng et al., 2020), we believe that the cellular mechanism of H_2

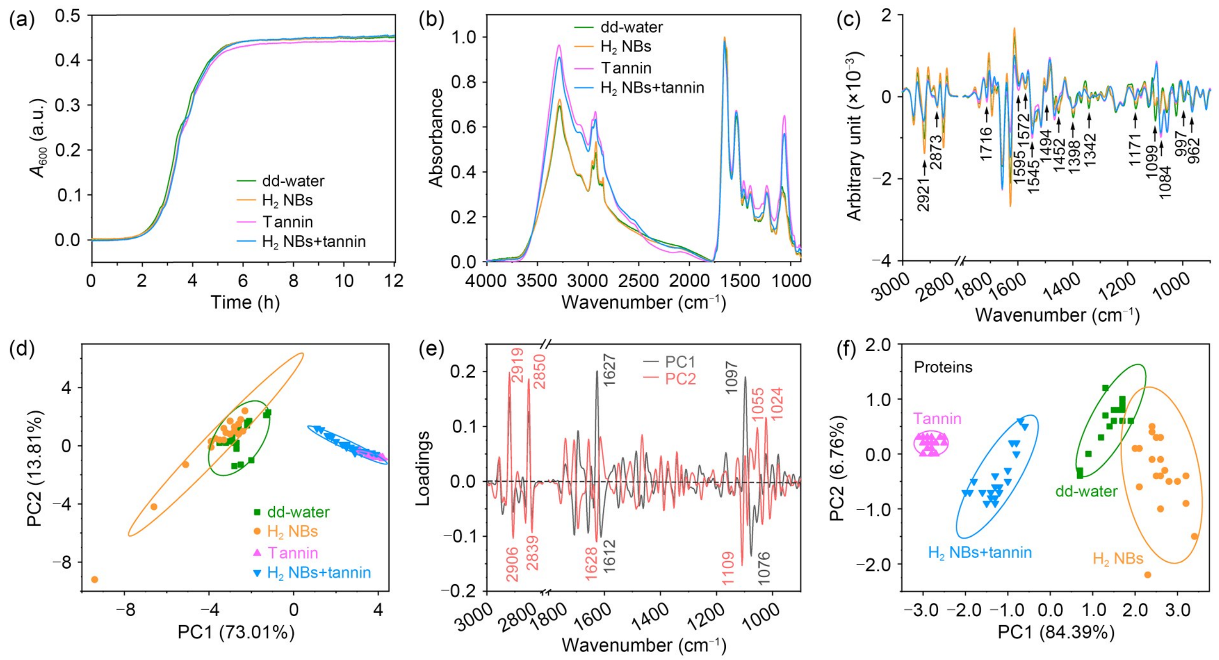

Fig. 3 Distinct biological effects between hydrogen (H_2) nanobubbles (NBs) and tannins on *Escherichia coli*. (a–c) Bacterial growth curves (a), Fourier transform infrared (FTIR) absorption spectra (b), and second-derivative spectra (c) of *E. coli*, where the arrows indicate significantly shifted bands; (d) Principal component analysis (PCA) on the second-derivative spectra (3000–2800 cm^{-1} and 1800–900 cm^{-1}) of *E. coli* (20 replicates each), where the ellipses represent 95% confidence interval (CI); (e) The corresponding loading values of PC1 (grey) and PC2 (red) from (d); (f) PCA on the second derivative spectra of bacteria in the protein region (1760–1480 cm^{-1}). dd-water: double distilled water; A_{600}: absorbance at 600 nm; a.u.: arbitrary unit.

molecule and/or NB is beyond being an antioxidant, i.e., H_2 might have other effects besides the widely described antioxidant effect. Thus, our findings provide a novel insight into the possible mechanism of action of molecular H_2, as well as other gases, at the cellular level. To our knowledge, this is the first report on the effects of H_2 on bacterial cells at the chemical molecular level in vitro, and in turn justifies further scientific endeavors in this direction.

Materials and methods

Detailed methods are provided in the electronic supplementary materials of this paper.

Acknowledgments

This work was supported by the National Natural Science Foundation of China (No. U1732130), the Key Research Program of Frontier Sciences of the Chinese Academy of Sciences (No. QYZDJSSW-SLH019), and the Yantai Region and College Integration Development Project (No. 2021XDRHXMPT28). We thank all the staff at the BL01B beamline of the National Facility for Protein Science in Shanghai (NFPS) at Shanghai Synchrotron Radiation Facility for the assistance during data collection.

Author contributions

Junhong LÜ designed the experiments and co-supervised the project with Bin LI and Jun HU. Jinfang LU, Jin ZHENG, Yadi WANG, and Jie CHENG performed the experiments. Junhong LÜ, Bin LI, and Xueling LI analyzed the data. Junhong LÜ, Jinfang LU, Jin ZHENG, and Yadi WANG wrote the manuscript. All authors have read and approved the final version of the manuscript, and therefore, have full access to all the data in the study and take responsibility for the integrity and security of the data.

Compliance with ethics guidelines

Jinfang LU, Jin ZHENG, Yadi WANG, Jie CHENG, Xueling LI, Jun HU, Bin LI, and Junhong LÜ declare that they have no conflict of interest.

This article does not contain any studies with human or animal subjects performed by any of the authors.

References

Alvarez-Ordóñez A, Mouwen DJM, López M, et al., 2011. Fourier transform infrared spectroscopy as a tool to characterize molecular composition and stress response in foodborne pathogenic bacteria. *J Microbiol Methods*, 84(3):369-378. https://doi.org/10.1016/j.mimet.2011.01.009

Bordoni L, Gabbianelli R, Fedeli D, et al., 2019. Positive effect of an electrolyzed reduced water on gut permeability, fecal microbiota and liver in an animal model of Parkinson's disease. *PLoS ONE*, 14(10):e0223238. https://doi.org/10.1371/journal.pone.0223238

Cheng J, Tang C, Li XL, et al., 2020. Hydrogen molecules can modulate enzymatic activity and structural properties of pepsin in vitro. *Colloids Surf B Biointerfaces*, 189:110856. https://doi.org/10.1016/j.colsurfb.2020.110856

Hu XJ, Liu ZX, Wang YD, et al., 2016. Synchrotron FTIR spectroscopy reveals molecular changes in *Escherichia coli* upon Cu^{2+} exposure. *Nucl Sci Tech*, 27:56. https://doi.org/10.1007/s41365-016-0067-9

LeBaron TW, Kura B, Kalocayova B, et al., 2019. A new approach for the prevention and treatment of cardiovascular disorders. Molecular hydrogen significantly reduces the effects of oxidative stress. *Molecules*, 24(11):2076. https://doi.org/10.3390/molecules24112076

Lee D, Park S, Bae S, et al., 2015. Hydrogen peroxide-activatable antioxidant prodrug as a targeted therapeutic agent for ischemia-reperfusion injury. *Sci Rep*, 5:16592. https://doi.org/10.1038/srep16592

Ohta S, 2015. Chapter fifteen—molecular hydrogen as a novel antioxidant: overview of the advantages of hydrogen for medical applications. *Methods Enzymol*, 555:289-317. https://doi.org/10.1016/bs.mie.2014.11.038

Ostojic SM, 2021. Hydrogen-rich water as a modulator of gut microbiota. *J Funct Foods*, 78:104360. https://doi.org/10.1016/j.jff.2021.104360

Qiu XC, Dong KS, Guan JZ, et al., 2020. Hydrogen attenuates radiation-induced intestinal damage by reducing oxidative stress and inflammatory response. *Int Immunopharmacol*, 84:106517. https://doi.org/10.1016/j.intimp.2020.106517

Sha JB, Zhang SS, Lu YM, et al., 2018. Effects of the long-term consumption of hydrogen-rich water on the antioxidant activity and the gut flora in female juvenile soccer players from Suzhou, China. *Med Gas Res*, 8(4):135-143. https://doi.org/10.4103/2045-9912.248263

Suzuki A, Ito M, Hamaguchi T, et al., 2018. Quantification of hydrogen production by intestinal bacteria that are specifically dysregulated in Parkinson's disease. *PLoS ONE*, 13(12):e0208313. https://doi.org/10.1371/journal.pone.0208313

Valdes AM, Walter J, Segal E, et al., 2018. Role of the gut microbiota in nutrition and health. *BMJ*, 361:k2179. https://doi.org/10.1136/bmj.k2179

Wang YD, Li XL, Liu ZX, et al., 2017. Discrimination of foodborne pathogenic bacteria using synchrotron FTIR microspectroscopy. *Nucl Sci Tech*, 28:49. https://doi.org/10.1007/s41365-017-0209-8

Yang ML, Dong YM, He QN, et al., 2020. Hydrogen: a novel option in human disease treatment. *Oxid Med Cell Longev*, 2020:8384742. https://doi.org/10.1155/2020/8384742

Supplementary information

Materials and methods; Figs. S1–S3